PASJ: Publ. Astron. Soc. Japan **46**, 147–154 (1994)

CO Observations of Edge-on Galaxies. IV. NGC 4565: Radial Variation of the H_2-to-H I Ratio

Yoshiaki SOFUE
Institute of Astronomy, The University of Tokyo, Mitaka, Tokyo 181
E-mail: sofue@sof.mtk.ioa.s.u-tokyo.ac.jp
and
Naomasa NAKAI
Nobeyama Radio Observatory, Minamimaki-mura, Minamisaku, Nagano 384-13*

(Received 1992 August 10; accepted 1993 November 17)

Abstract

The edge-on galaxy NGC 4565 has been observed in the ^{12}CO ($J=1$–0)-line emission using the Nobeyama 45-m telescope with an angular resolution of 15″. We obtained a scan along the major axis for ±5′(±15 kpc) about the galactic center, and some scans perpendicular to the galactic plane. The radial density distribution shows a dense molecular gas ring of 5 kpc radius, which is associated with an H I ring. The molecular disk comprises two components: an unresolved thin and dense disk, and a thick disk (or a halo) extending to a height greater than 1.4 kpc. The position-velocity diagram shows that the general rotation of the entire galaxy is circular with a flat rotation curve. However, the radial distribution of molecular gas is asymmetric with respect to the galaxy center in the sense that the molecular gas is much richer in the NW side. We derived a radial variation of the H_2-to-(H I+H_2) density ratio, and found that interstellar gas in the central 4 kpc region is almost entirely H_2, while H I is dominant beyond 10 kpc. A similar H I-vs-H_2 behavior was found in the edge-on galaxy NGC 891.

Key words: CO emission — Edge-on galaxies — Galaxies — Molecular hydrogen

1. Introduction

NGC 4565 is a nearby Sb galaxy having a large angular size with a nearly edge-on orientation at an inclination angle of 86°, and has been extensively studied by optical observations (de Vaucouleurs 1958; Frankston, Schild 1976; Hamabe et al. 1980; van der Kruit, Searle 1981). A sharp, straight dark lane runs along the galactic plane (e.g., Sandage 1961), indicating the presense of a significant amount of interstellar dust and, therefore, a significant amount of molecular gas. CO line observations using the 7-m telescope at an angular resolution of 100″ indicated a centrally peaked molecular gas disk (Richmond, Knapp 1986). The galaxy has also been observed in the radio continuum at various frequencies, which reveals a thin disk of nonthermal as well as thermal emissions (Hummel et al. 1984). Observations of the H I line emission have shown a large disk of interstellar gas, which is warping in the outermost regions (Sancisi 1976; Rots 1980; Rupen 1990).

Edge-on galaxies provide a unique opportunity to investigate the major-axis distribution of interstellar gas as well as the distribution perpendicular to the galactic plane. However, since the CO emission in NGC 4565 is relatively weak compared to that of other galaxies like NGC 891, there has been no high-resolution observations in the CO line, and no detailed kinematical characteristics of the molecular gas has been investigated.

This paper is the fourth in a series describing the results of a high-resolution, high-sensitivity survey of edge-on galaxies in the ^{12}CO ($J=1$–0) line using the Nobeyama 45-m telescope. In Papers I (Sofue et al. 1987) and III (Sofue, Nakai 1992) we presented results for edge-on galaxy NGC 891, and in Paper II (Sofue et al. 1989) and in Sofue et al. (1990) we described results for NGC 4631. In the present paper, we describe the results for NGC 4565.

2. Observations

Observations of the ^{12}CO ($J=1$–0) line emission of NGC 4565 were performed in 1992 January and 1992 December using the 45-m telescope of the Nobeyama Radio Observatory in the course of a CO-line survey of edge-on galaxies. The parameters for NGC 4565 are given in table 1. The systemic LSR velocity is taken to be 1225 km s^{-1} according to the H I helio-centric velocity

* NRO is a branch of the National Astronomical Observatory, an inter-university research institute operated by the Ministry of Education, Science and Culture.

Table 1. Parameters for NGC 4565.

The center position ($X = 0''$, $Y = 0''$)		NED*
R.A.$_{1950}$	$12^h33^m51^s.8$	
Decl.$_{1950}$	$26°15'50''.0$	
PA of the major axis	135.°5	Rupen (1990)
Systemic velocity ($V_{\rm LSR}$)	1230 ($\pm$5) km s^{-1}	Present CO result
$V_{\rm rot}$	250 ($\pm$5) km s^{-1}	Present CO result
Distance	10.2 Mpc	Schöniger, Sofue (1993)

* NASA/IPAC Extragalactic Database (1991) (operated by Jet Propulsion Laboratory, California Institute of Technology under contract by NASA).

of 1230 km s^{-1} (Sancisi 1976). We adopt a distance of 10.2 Mpc, which was derived by using the Tully-Fisher relation by Schöniger and Sofue (1993). This value is consistent with the value suggested by de Vaucouleurs (see Richmond, Knapp 1986; Rupen 1990). Hence, the linear scale at the galaxy corresponds to $1' = 3.0$ kpc.

Since the observational parameters are described in Paper III, we summarize them only briefly. The antenna had a HPBW of 15″, which corresponds to a linear resolution of 742 pc. The aperture and main-beam efficiencies of the telescope were $\eta_{\rm A} = 0.35$ and $\eta_{\rm mb} = 0.50$, respectively. We used an SIS receiver combined with a 2048-channel acousto-optical spectrometer of 250 MHz bandwidth corresponding to a velocity coverage of 650 km s^{-1}. After binding up every 32 channels in order to increase the signal-to-noise ratio, we obtained spectra with a velocity resolution of 10.2 km s^{-1}. The system noise temperatue was 600 to 800 K at observing elevations in the observations in 1992 January, and 400 to 500 K in December. We used a multi-on-off switching mode, with which we observed six on-source positions and two off positions at 5′ to the east and west in a single sequence of observing runs.

The intensity scale used in the observations was the antenna temparature $T_{\rm A}^*$, which is converted to the main-beam brightness temperature by $T_{\rm mb} = T_{\rm A}^*/\eta_{\rm mb} = 2.0T_{\rm A}^*$; we use $T_{\rm mb}$ in this paper. The on-source total integration time was about 5 to 10 minutes per each point. The rms noise of the resultant spectra at 10 km s^{-1} resolution is typically 20 mK in $T_{\rm mb}$. The pointing of the antenna was calibrated every 1 to 1.5 hours using a nearby SiO maser star at 43 GHz; the pointing accuracy through the obsevations was better than ±3″.

We used a coordinate system (X, Y), in which X and Y are defined as the distances along the major and minor axes from the center position, respectively (X is positive toward the south-east, and Y is positive toward the north-east perpendicular to the X-axis). Observations were made at every 15″ grid interval along the major axis from $X = -5'$ to $+5'$. Since the grid interval was equal to the HPBW of the antenna, the data were undersampled, so that the final data gave an effective angular resolution of $\theta = ({\rm HPBW}^2 + \Delta X^2)^{1/2} = 21''$. Additional observations were made at several positions in the Y direction at $X = \pm 2'$ and $\pm 3'$, by which we confirmed that the CO intensity had a sharp maximum near to the major axis. We adopted the position angle of the major axis to be 135.°5 after Rupen (1990), and used it in the observations in 1992 December. However, we used a position angle of 139° in the observations in 1992 January. These yielded two sets of data, which referred to slightly different coordinate systems inclined by a few degrees from each other. Since the observing points were distributed in a complex way, we combined them so as to obtain a set of spectra along the major axis at PA = 135.°5, and made use of them to produce a position-velocity diagram. This diagram practically contains almost all of the information which we obtained from the observations.

3. Results

3.1. Position-Velocity Diagram

We made use of a composite set of obtained spectra to produce a position-velocity (PV) diagram along the major axis at 135.°5. Thereby, we convolved the data with a Gaussian beam with HPBW=20″ in the X and Y directions. The obatained position-velocity (PV) diagram is shown in figure 1. The data were also smoothed in velocity to a velocity resolution of 20 km s^{-1}. This yielded an rms noise of about 12 mK in $T_{\rm mb}$ on the PV map; the contours in figure 1 are drawn at every 40 mK in $T_{\rm mb}$.

The PV diagram provides various information concerning the kinematics of the galaxy, particularly rotation. A rigid rotation feature is observed at $|X| < 1'$. The intensity ridge at $-1' < X < 1'$ can be well defined by an apparently-rigid rotation feature which has two maxima at $X = \pm 30''$ (1.5 kpc) and $V_{\rm LSR} \sim 1180$ and ~ 1300 km s^{-1}, respectively.

In the outer region beyond $X \sim \pm 1'$, the rotation velocity is almost constant, indicating a flat rotation curve. By simply tracing the intensity maxima on the

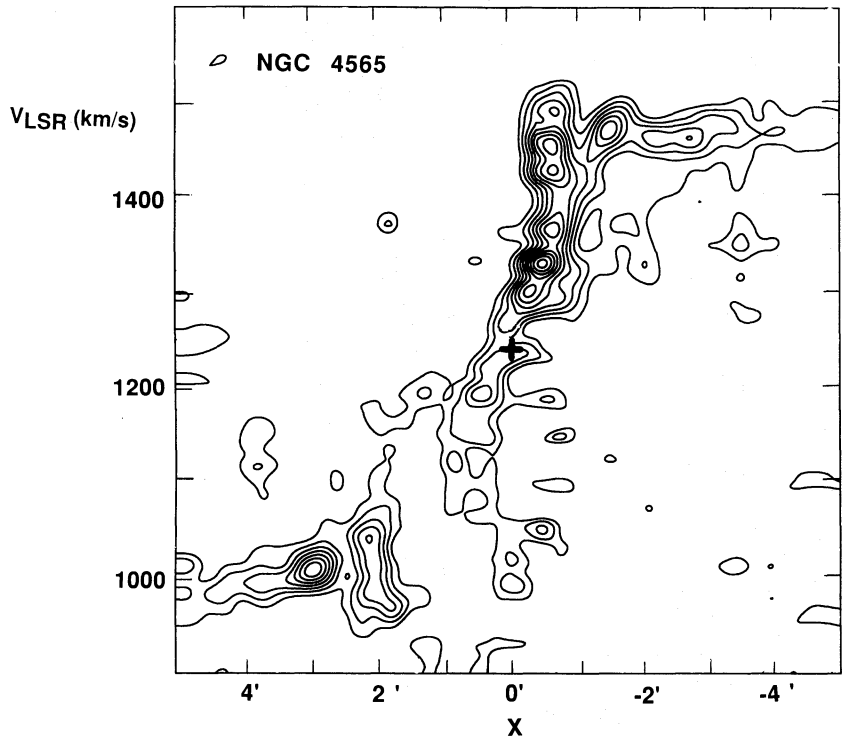

Fig. 1. Position-velocity ($X - V$) diagram along the major axis of NGC 4565. The resolution in the map is $\Delta X \times \Delta V = 20'' \times 20$ km s^{-1}, and the effective rms noise of the map is about 12 mK in $T_{\rm mb}$. Contours are drawn at every 40 mK in $T_{\rm mb}$ starting at 40 mK, and the peak intensity in the map is 420 mK in $T_{\rm mb}$. The cross marks the galaxy center and the systemic velocity.

PV diagram, we find that a flat rotation occurs at $V_{\rm LSR}$ = 1480 km s^{-1} and 980 km s^{-1}, which yields a rotation velocity of 250($\pm$10) km s^{-1}. This rotation velocity is in a good agreement with the H I rotation velocity (255 km s^{-1}; Rupen 1990). From these results we can also derive a systemic velocity of 1230 ± 5 km s^{-1}, which is in a good agreement with the H I systemic velocity (1225 km s^{-1}; Rupen 1990). Hence, regardless of the significant asymmetry in the gas distribution, the galaxy is rotating regularly at a constant velocity of 250 km s^{-1} symmetrically about its systemic velocity (1230 km s^{-1}). Such a regular rotation is reasonable in view of the isolation of NGC 4565 from other galaxies.

In addition to these features, a high-velocity component is seen near to the center at $X \sim -30''$ and $V \sim$ 1400–1500 km s^{-1}, while its opposite counterpart is lacking, or is very weak. This feature could be interpreted as being due to a nuclear disk or ring with a radius of 1.5 kpc, whose distribution is highly asymmetric with respect to the center.

3.2. *Total Line Profile*

Figure 2 shows a "total line profile" in CO for NGC 4565, which was obtained by integrating the spectra along the major axis at $-5' < X < 5'$, or equivalently by integrating the PV diagram in the X direction. We find a good coincidence with the result obtained by Richmond and Knapp (1986). The "lopsidedness" of the CO gas distribution, namely the much stronger emission in the positive-velocity side in NW ($X < 0'$) than in the negative-velocity side in SE, is also reproduced in this total profile.

In figure 2 we superpose an H I line profile taken from Rots (1980). The H I and CO line profiles coincide well with each other. The total velocity width at the 20% level of the peak intensity was measured to be 540 ± 10 km s^{-1}, and is about equal to that obtained for the H I emission of 520 to 535 km s^{-1} (Rots 1980; Rupen 1990). This fact supports the argument that the total CO line profiles of galaxies can be used as an alternative to the H I Tully-Fisher (1977) relation, as has been discussed in the case of NGC 891 (Sofue, Nakai 1992) and for other galaxies (Dickey, Kazes 1992; Sofue 1992; Schöniger, Sofue 1993).

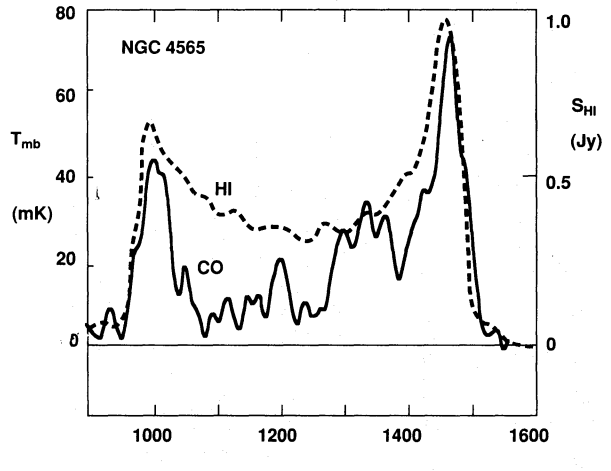

Fig. 2. Total line profile of the ^{12}CO ($J=1$–0) emission along the major axis. The velocity resolution in this diagram is 10 km s^{-1}. An H I total line profile is indicated by the dashed line (Rots 1980).

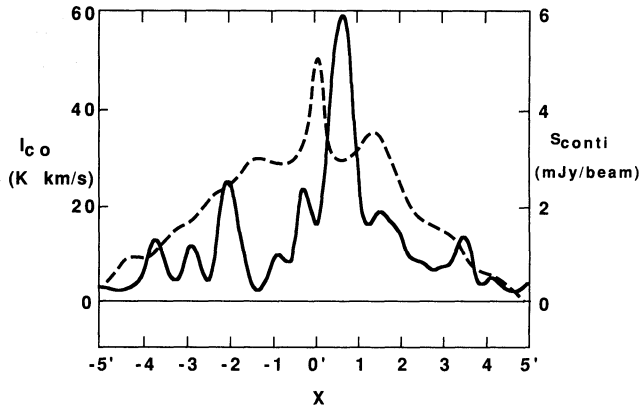

Fig. 3. I_{CO} distribution along the major axis X (full line), and intensity of 20-cm continuum emission (dashed line: Sukumar, Allen 1991). The resolution in the X direction is 20″.

3.3. *Intensity Distribution*

The distribution of the integrated intensity, $I_{CO} = \int T_{mb} dV$, can be obtained by integrating the intensity in figure 1 in the direction of the velocity; it is shown in figure 3 as a function of X. The figure indicates a general concentration of CO gas toward the center. The central strong peak, as observed with the 100″ resolution (Richmond, Knapp 1986), has been resolved into two peaks at $X \simeq \pm 30''$ in our observation. The peaks observed $X = \pm 3'$ by Richmond, Knapp (1986) coincide with several peaks at $X = \pm 2$–$3'$, and finer structures are present. Also apparent in this figure is the asymmetry of the intensity: it is much stronger in the NW disk than in the SE disk. It is interesting to note that this asymmetry is consistent with the asymmetry of dust lane distributions on the optical photographs (de Vaucouleurs 1958; Hamabe et al. 1980), although optical data indicate only foreground absorbing clouds, which not necessarily represent the total dust distribution.

The distribution of radio continuum emission at 20 cm along the major axis is reproduced from Sukumar, Allen (1991), and indicated by the dashed line in figure 3. Although we find some global correlation, CO and continuum emissions seem to be not well correlated in a few kpc scale length. In particular, the CO emission seems to avoid the nuclear continuum source. Since the 20-cm continuum is dominated by nonthermal emission, it is not adequate to compare these in the scheme of star-formation efficiency, as we did for NGC 891 using the 6-cm continuum (Sofue, Nakai 1992).

3.4. *Molecular Mass*

By integrating all of the CO emission in figure 3 we can estimate the total luminosity in the ^{12}CO ($J=1$–0) emission along the major axis: The total CO luminosity for the observed region at $-5' < X < 5'$ and $-7\farcs5 < Y < 7\farcs5$ (within ± 15 kpc radius and ± 370 pc thickness) is estimated to be $L_{CO} = 4.2\ (\pm 0.4) \times 10^8$ K km s^{-1}pc^2. The error has been estimated as $\delta L = [40\,(\text{number of observed points})]^{1/2} \times \delta L$ (individual spectrum), where δL (individual spectrum) $= 3\,\delta T_{mb}$ (rms) $\delta V \sqrt{N}$ and $N = 650$ km s^{-1}/10 km s^{-1} $= 65$.

If we assume an H_2 column density-to-CO intensity conversion factor of $C = 3.6 \times 10^{20}$ H_2 cm^{-2}/K km s^{-1} (Sanders et al. 1984), the luminosity can be related to the mass as $M_{H_2} = 5.7\ L_{CO}$. Then, the total mass of H_2 gas within the thin disk of 15 kpc radius is estimated to be $M_{H_2} = 2.4(\pm 0.2) \times 10^9\ M_\odot$. [If we take a smaller conversion factor of 2.8×10^{20} H_2 cm^{-2}/K km s^{-1} (Bloemen et al. 1985), the estimate of the molecular gas mass should be reduced by a factor of $2.8/3.6 = 0.78$.] Thus the estimated mass is less than the molecular mass obtained by Richmond, Knapp (1986) ($\sim 6 \times 10^9\ M_\odot$ for the same conversion factor). This discrepancy may be due to the wider coverage by Richmond, Knapp's observations along the major axis ($-13' < X < 15'$; or $-39 < X < 45$ kpc) as well as to their wider beam (100″ = 5 kpc), with which they possibly detected CO in the halo or a thick-disk (see subsection 3.8).

3.5. *Radial Density Distribution of the Gas Disk for a Flat Rotation Curve*

The rotation curve of NGC 4565 is flat and the rotation velocity of the galaxy is about 250 km s^{-1}. Using this fact, we can derive an approximate radial distribution of

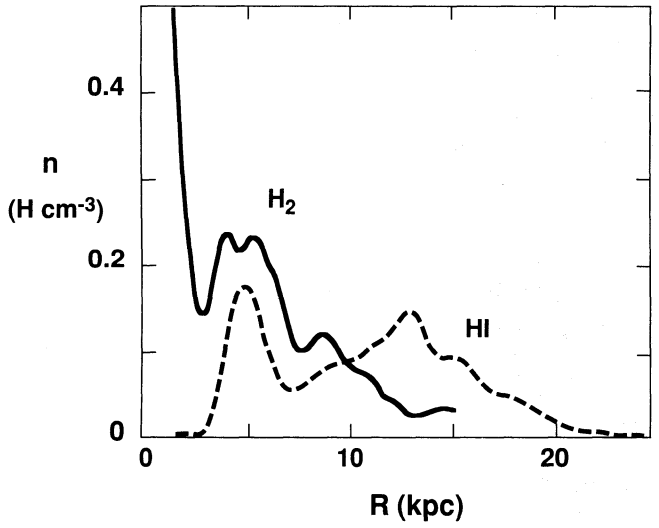

Fig. 4. Beam-diluted spatial densities of molecular and neutral hydrogen gases (in H cm^{-3}), averaged in the Y-direction by a beam size of 20″ (1 kpc).

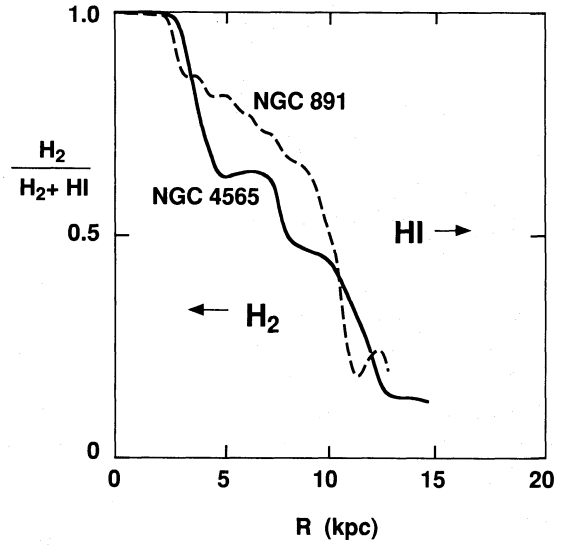

Fig. 5. Mass ratio of H_2 to the total (H I+H_2) gas density as a function of the galactocentric distance.

the gaseous density for the flat-rotation part of the disk [see Paper III (Sofue, Nakai 1992) for detail]. According to Paper III, the gas density at radius $R = |X|$ can be obtained approximately by

$$n_{H_2} = CI_{CO}/l, \quad (1)$$

where

$$l = 2|X|\sqrt{V_{rot}^2/V_{min}^2 - 1}. \quad (2)$$

Here, V_{min} is the minimum rotation velocity for the integration of I_{CO}, and V_{rot} is the rotation velocity, I_{CO} is the integrated intensity around V_{rot}, which is obtained by integrating T_{mb} for a range of $V_{min} < |V_{LSR} - V_{sys}| < V_{max}$. We take $V_{min} = 200$ and $V_{max} = 280$, which leads to $l = 1.5|X|$. We note that the spatial density obtained by equation (1) indicates a beam-diluted density, or a density averaged in the Y direction (perpendicular to the galactic plane) by the beam width (20″ = 1 kpc). Since the molecular gas layer must be much thinner, the true density should be several times greater than the value indicated here; for example, if we assume 100 pc thickness, the true density can be obtained by multiplying by a factor 10.

Figure 4 shows the thus-obtained distribution of spatial density of H_2 (n_{H_2} in H cm^{-3}) as a function of the radius. The distribution of n_{H_2} indicates a concentration of H_2 gas at a radius of 5 kpc. This fact indicates either that the gas distribution is ring-like, or that dense spiral arms run at this radius. Since our observations do not tell about the arm structures, we here simply interpret this as being due to a ring-like (although broad) distribution of molecular gas. Figure 4 also shows another strong concentration of molecular gas near the center, although error and uncertainty of the derived value are large in the central few kpc. This central enhancement is due to a possible nuclear disk, which can be seen in the PV diagram (figure 1).

We apply the same method to an H I intensity distribution in the edge channels ($V_{min} = 240$, $V_{max} = 280$) around the terminal velocity as obtained by Rupen (1991) using their 20″ resolution data. In figure 4 we plot thus obtained H I density by a dashed line. Density indicated here represents also a beam-diluted value, averaged in the Y direction by the 20″ (= 1 kpc) H I beam. The H I density tends to zero inside a 4 kpc radius, while it has a sharp ring at a 5 kpc radius followed by a broad outer ring-like distribution with the second peak at 13 kpc radius. The total H I+H_2 density has a clear ring structure at $R \sim 4$–5 kpc. The H_2 molecules are present mainly inside a 10 kpc radius, while H I gas has a broad outskirt reaching as far as a 22 kpc radius.

3.6. *H I-to-H_2 Gas Ratio*

As shown in figure 4, the H I and H_2 gases seem to be present at different radii, gradually avoiding each other. Figure 5 plots the mass ratio of the H_2 gas density to the total (H I+H_2) gas density, as obtained by using figure 4. The H I gas is dominant in the outer region beyond 7 kpc, while H_2 is dominant in the inner region. Particularly for the inner 4 kpc region, the gas is almost totally molecular. The "exchange" from H I to H_2 appears to occur in

coincidence with the molecular gas ring at 5 kpc radius.

For a comparison, we plot the $H_2/(HI+H_2)$ ratio obtained for the edge-on galaxy NGC 891 by the dashed line in figure 5, which was calculated from the radial HI and H_2 distributions obtained by Sofue, Nakai (1992). A similar radial behavior is seen for the exchange from HI to H_2 at around 8–10 kpc radius. The HI-to-H_2 exchange also occurs in this galaxy at 3 kpc, coinciding with its 3.4 kpc molecualr ring, inside which the gas is almost perfectly molecular.

We may be able to interpret this diagram in terms of an evolutionary scenario of interstellar gases in spiral galaxies as follows. We may suppose that a primeval galaxy was born as a rotating gaseous disk, which comprised primeval HI. Due to the higher gas density in the innermost region of the galaxy, the initial star-formation activity was triggered near to the nucleus. This resulted in an increase in the metal abundance in the central region, and, therefore, to an increase in the circum-stellar formation rate of dust grains. It is then followed by an increase in interstellar dusts, as represented by far-IR observations (Wainscoat et al. 1987). According to the increase in dust grains, interstellar hydrogen is transformed to H_2 molecules through catalystic actions on grain surfaces (e.g., Shull, Beckwith 1982). The action rate is obviously higher near to the center according to the higher metal abundance. Hence, the HI gas in the central region is more rapidly transformed to H_2, and therefore to molecular clouds, than that in the outer region. Particularly, in the innermost region (inside the molecular rings: $r < 4$ kpc for NGC 4565; 3 kpc for NGC 891) the rate was sufficiently high to transform the gas to H_2 almost entirely, while it was not so high at distances larger than 10 kpc from the center, and the gas remains to be HI.

Another effect to maintain the higher H_2-to-HI ratio in the central region is an increase in the column density of hydrogen molecules and dust grains: self-shielding by H_2 molecules and absorption by dust prevent UV radiation from penetrating deep into molecular clouds, and, thus, the dissociation of H_2 into HI is suppressed, particularly, within $r < 4$ kpc.

3.7. The Molecular Gas Ring

Figure 4 indicates an intensity peak at $X \simeq 5$ kpc; we interpreted this peak as being due to a ring of molecular hydrogen gas. Hereafter, we call this intensity peak the molecular gas "ring," although a ring and arms cannot be distinguished from each other since no informatin about a face-on distribution is available. A similar concentration of molecular gas at radii of 4 to 5 kpc has been observed in other edge-on galaxies so far resolved in CO, and seem to be a common characteristics of spiral galaxies. For example, NGC 891 has a ring with a radius of about 3 kpc (Sofue, Nakai 1992); the Milky Way has the 4-kpc molecular ring (Dame et al. 1987).

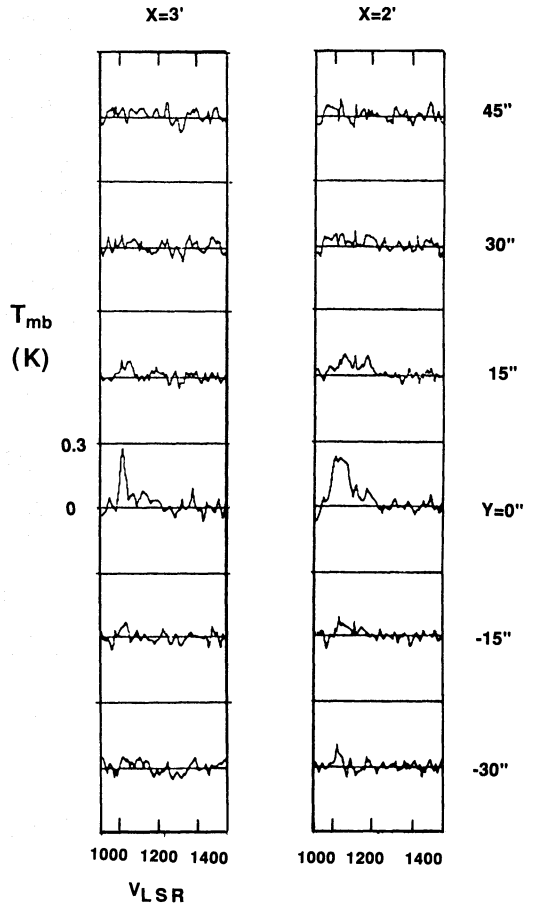

Fig. 6. ^{12}CO ($J=1$–0) spectra at various heights (Y) from the galactic plane at $X = 2'$ and $3'$.

Nakai (1992) has suggested that such a molecular gas ring is characteristic for a barred spiral galaxy. NGC 4565 has a box- or peanut-shaped bulge (Kormendy, Illingworth 1982), and such a shape is suggested to have been sustained by a stellar bar (Combes, Sanders 1981; Combes et al. 1990). We may thus conjecture that NGC 4565 could be classified as being SBb, rather than a normal Sb.

3.8. Disk Thickness

In order to clarify whether our observations could cover a substantial fraction of the total emission in the Y direction, or if the molecular gas is extended in a thicker disk so that we missed some fraction, we obtained some scans perpendicular to the disk plane. Figure 6 shows an example of spectra taken at $X = 2'$ and $3'$ at several heights (Y) perpendicular to the X-axis. The figure indicates that, although the CO intensity decreases rapidly with the height, weak emission can be seen above

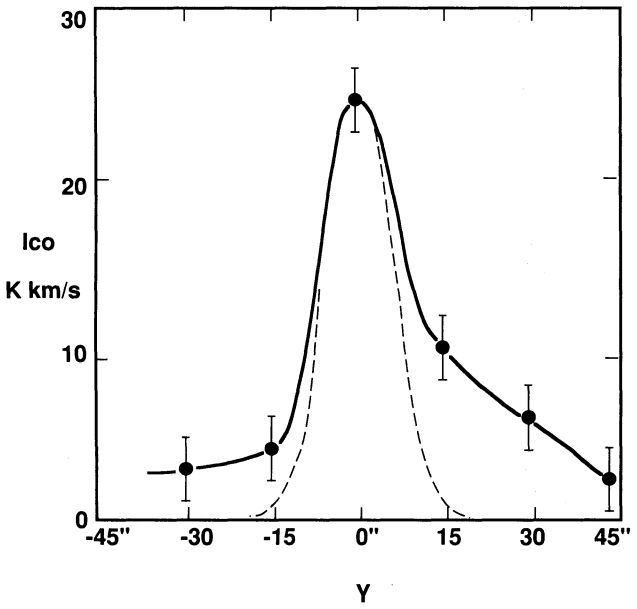

Fig. 7. CO intensity distribution perpendicular to the galactic plane at $X = +2'$ as a function of Y. The distribution comprises two components: a thin and dense disk, and an extended thick disk or a halo. The dashed line represents a Gaussian beam with HPBW=15″.

$Y \simeq \pm 15''$. Figure 7 shows a plot of the integrated CO intensity across the galactic plane (as a function of Y) at $X = +2'$. This figure indicates that significant emission is detected beyond $Y \sim \pm 15''$. This fact shows that the molecular gas distribution comprises two components: a thin and dense disk, whose thickness is smaller than the beam size (0.7 kpc), and a thick diffuse disk (or a halo), which extends at least up to $Y \sim \pm 30$–$45''$ with a scale height greater than 1.4 kpc. The emission from the extended component is comparable to that from the galactic plane covered by our 15″ beam.

Using the intensity distribution along the major axis obtained by Richmond, Knapp (1986) with their 100″ beam, we estimated the "total" H_2 mass within $-5' < X < 5'$ to be $\sim 5 \times 10^9\ M_\odot$, which is the mass contained within an area of $10' \times 100'' = (30\ \mathrm{kpc} \times 5\ \mathrm{kpc})$. This mass is significantly greater than the presently derived mass of $2.4(\pm 0.2) \times 10^9 M_\odot$ along the galactic plane within $10' \times 15''$ (30 kpc × 0.74 kpc) in subsection 3.4. This discrepancy may imply that a substantial fraction of H_2 mass (the rest $\sim 2.6 \times 10^9\ M_\odot$) is distributed beyond the thin disk that was covered by the present beam of 15″ HPBW. This is consistent with the extended emission, as shown in figure 7. The dynamical mass of the galaxy within a radius $r = 15$ kpc can be estimated to be $M_{\mathrm{dyn}} \sim 2.0 \times 10^{11}\ M_\odot$ from a rotation velocity of 250 km s^{-1}. Hence, if we include the thick-disk component, approximately 2.5% of the total mass is taken by the molecular gas within the same radius, while only 1% is taken by the thin molecular disk of thickness less than 0.7 kpc (15″).

Alternatively, the apparently extended component beyond $Y \sim \pm 15''$ could be explained by a tilted disk by 4° from the line of sight (de Vaucouleurs 1958), even if the disk thickness is sufficiently small. For example, emission from the disk plane at 10 and 20 kpc distance from the major axis (node) is observed at $Y \sim \pm 0.7$ and 1.4 kpc, respectively. In this case, the radial velocity of the emission should vary with the distance and, therefore, with Y: the larger is $|Y|$, the closer is the radial velocity to the systemic velocity. However, a careful inspection of figure 6 reveals no such variation of the radial velocity with Y, at least up to $Y \sim \pm 30$–$45''$, but it does indicate a corotation of the extended component with the disk gas. Hence, we may conclude that the extended emission in figure 7, and probably the larger amount of molecular gas observed by larger beam of 100″ by Richmond, Knapp (1986), is due to an extended molecular gas halo or thick disk.

4. Summary

We mapped the major axis of the edge-on galaxy NGC 4565 in the ^{12}CO ($J = 1$–0) line emission using the Nobeyama 45-m telescope at an angular resolution of 15″ (= 742 pc). The results are summarized as follows:

(a) The position-velocity diagram indicates a flat rotation of the galaxy disk, and its rotation characteristic is symmetric with respect to the galactic center as well as to the systemic velocity. The rotation velocity of the flat part is 250 km s^{-1}. Although the general rotation is symmetric, the molecular gas distribution is asymmetric with respect to the galactic center.

(b) The molecular mass involved in the thin disk within 15 kpc radius is estimated to be $2.4\ (\pm 0.2) \times 10^9\ M_\odot$, which takes only 1% of the total (dynamical) mass within the same radius. In addition to the thin and dense disk, a comparable amount of molecular gas is present in a thick disk or halo with a scale height greater than 1.4 kpc.

(c) The intensity and radial density distributions along the galactic plane shows a central condensation of molecular gas with rigid rotation, and a ring-like distribution at 5 kpc radius. This 5-kpc molecular ring is associated with an HI ring, followed by an outer extended HI disk.

(d) The H_2-to-(HI+H_2) mass ratio increases toward the center. Interstellar gas in the innermost region at $R < 4$ kpc is almost entirely molecular, while it is HI dominant outside 10 kpc radius, and the HI to H_2 exchange occurs at around 4 kpc just at the inner edge of the 5-kpc ring. The diagram could be interpreted as representing a histroy of the overall conversion of HI to H_2 in a disk galaxy, and should be useful for a discus-

sion concerning an evolution of interstellar gas in a disk galaxy.

The authors thank the staff of NRO for their help during the observations.

References

Bloemen J.B.G.M., Strong A.W., Blitz L., Cohen R.S., Dame T.M., Grabelsky D.A., Hermsen W., Lebrun F. et al. 1986, A&A 154, 25
Combes F., Debbasch F., Friedli D., Pfenniger D. 1990, A&A 233, 82
Combes F., Sanders R.H. 1981, A&A 96, 164
Dame T.M., Ungerechts H., Cohen R.S., de Geus E.J., Grenier I.A., May J., Murphy D.C., Nyman L.-A. et al. 1987, ApJ 322, 706
de Vaucouleurs G. 1958, ApJ 127, 487
Dickey J., Kazes I. 1992, ApJ 393, 530
Frankston M., Schild R. 1976, AJ 81, 500
Hamabe M., Kodaira K., Okamura S., Takase B. 1980, PASJ 32, 197
Handa T., Nakai N., Sofue Y., Hayashi M. Fujimoto M. 1990, PASJ 42, 1
Hummel E., Sancisi R., Ekers R.D. 1984, A&A 133, 1
Huntley J.M., Sanders R.H., Roberts W.W.Jr 1978, ApJ 221, 521
Kormendy J., Illingworth G. 1982, ApJ 256, 460
Nakai N.1992, PASJ 44, L27
Richmond M.W., Knapp G.R. 1986, AJ 91, 517
Rots A. 1980, A&AS 41, 189
Rupen M.P. 1991, AJ 102, 48
Sancisi R. 1976, A&A 53, 159
Sandage A.R. 1961, The Hubble Atlas of Galaxies (Carnegie Institution, Washington) p25
Sanders D.B., Solomon P.M., Scoville N.Z. 1984, ApJ 276, 182
Schöniger F., Sofue Y. 1993, A&A in press
Shull J.M., Beckwith S. 1982, ARA&A 20, 163
Sofue Y. 1992, PASJ 44, L231
Sofue Y., Handa T., Nakai N. 1989, PASJ 41, 937 (Paper II).
Sofue Y., Handa T., Golla G., Wielebinski R. 1990, PASJ 42, 745.
Sofue Y., Nakai N. 1992, PASJ 45, 139 (Paper III)
Sofue Y., Nakai N., Handa T. 1987, PASJ 39, 47 (Paper I)
Sørensen S.-A., Matsuda T., Fujimoto M. 1976, Ap&SS 43, 491
Sukumar S., Allen R.J. 1991, ApJ 382, 100
Tully B., Fisher J.R. 1977, A&A 54, 661
van der Kruit P.C., Searle L. 1981, A&A 95, 105
Wainscoat R.J., de Jong T., Wesselius P.R. 1987, A&A 181, 225